ARQII Publication
http://arqiipubl.com/ams
APPLICATIONS OF
MODELLING AND SIMULATION
eISSN 2600-8084
VOL 9, 2025, 174-188

Biological and Optimal Control Model for Powdery Mildew Disease in Mango Plants and Fruits

K. Vaishnavi and R. Malinidevi*

PG & Research Department of Mathematics, The Standard Fireworks Rajaratnam College for Women (Affiliated to Madurai Kamaraj University), Thiruthangal Road, Sivakasi-626123, Tamilnadu, India

*Corresponding author: malinidevi-mat@sfrcollege.edu.in

Submitted 12 January 2025; Revised 14 April 2025; Accepted 25 April 2025; Available online 10 May 2025.

Abstract: Powdery mildew is a major threat to mango plants, leading to significant agricultural and financial losses. This study introduces innovative mathematical models to capture the dynamics of powdery mildew infection in mango fruits and proposes an optimal control strategy to minimize disease spread and treatment costs. By applying advanced asymptotic techniques, such as the New Homotopy Perturbation Method, Adomian Decomposition Method, and Variational Iteration Method, this research derives novel approximate analytical solutions, which are rigorously validated against numerical results. The developed models offer a robust framework for understanding the disease dynamics and optimizing biological control measures, with a focus on minimizing both disease transmission and treatment expenses. The results demonstrate the efficacy and accuracy of these approaches, providing valuable insights into pest management strategies in mango cultivation.

Keywords: Analytical expression**;** Mango plant**;** Mathematical modelling; Optimal control; Powdery mildew.

1. INTRODUCTION

Powdery mildew is a widespread and destructive fungal disease that impacts a diverse range of plants, including mangoes (Mangifera indica). This disease is caused by the fungal pathogen *Oidium mangiferae*, a member of the *Erysiphaceae* family, which thrives in conditions of high humidity and moderate temperatures. It manifests mango plants and fruits as a white, powdery fungal growth on the surfaces of leaves, flowers, and fruits. The disease significantly reduces fruit yield and quality, posing a serious threat to mango cultivation, especially in regions where mango is a key agricultural product. The fungus *Oidium mangiferae* features hyaline, septate hyphae that produce conidia in chains, which are characteristic of its structure. The conidia of *Oidium mangiferae* are ellipsoid to cylindrical and can germinate rapidly to infect host tissues. The pathogen primarily targets young tissues such as panicles, leaves, and fruits, penetrating the epidermal cells to establish a parasitic relationship [1]. Its high reproductive capacity and swift infection cycle make it a serious threat to mango plantations. The disease appears as a whitish, powdery coating on panicles, leaves, and young fruits, leading to browning and defoliation [2]. Infected inflorescences often cause fruit abortion, and the remaining fruits may develop a scabby appearance. This disease has been reported in several regions, including Japan, Mexico, Israel, Egypt, and Spain.

Managing powdery mildew effectively involves the use of fungicides and integrated pest management strategies. In Israel, fungicides like penconazole, myclobutanil, and tetraconazole have proven effective, particularly when applied before rainfall [3]. In Egypt, integrated approaches combining biological control agents, mineral salts, and antioxidants have shown promise in reducing disease severity [4]. The use of phosphate fertilizers alongside systemic fungicides has also demonstrated success, cutting fungicide applications by up to 50% [5]. Current research on mango powdery mildew focuses on understanding the pathogen's biology, host-pathogen interactions, and developing effective control measures [6]. Advances in molecular biology are enabling researchers to explore the genetic mechanisms behind pathogen virulence and host resistance [7]. Mathematical modeling has become a valuable tool for simulating the spread and dynamics of powdery mildew, supporting the development of optimized management strategies. However, there is still a need for comprehensive models that integrate biological control measures, disease dynamics, and cost-effectiveness. Kumar *et al.* developed a predictive model using a hybrid CNN-Random framework to classify powdery mildew disease with high accuracy [8]. Kulkarni *et al.* demonstrated effective management techniques using organic products [9]. Nalawade *et al.* created a disease detection model leveraging artificial neural networks [10]. In Egypt, Ahmed *et al.* conducted experimental analyses to evaluate the effectiveness of bio-control agents in managing powdery mildew [11].

Numerous researchers have developed mathematical models to study powdery mildew across various plant species. For instance, a disease evaluation model utilizing the Expectation-Maximization (EM) algorithm and Gaussian mixture has been

designed for field detection using smart-phones, offering practical on-site utility [12]. To monitor powdery mildew in wheat, the CARS-ELM model was created using remote sensing data, alongside image processing techniques that identified leaf-level infections with 93.33% accuracy [13]. In rubber trees, early detection has been enhanced using wavelet-based models, improving detection efficiency by 1.9% [14]. Similarly, machine learning models have been developed to classify infected sandalwood trees based on environmental variables such as humidity, temperature, and soil moisture [15]. In recent years, mathematical models based on differential equations have also emerged to study powdery mildew dynamics in various crops. Notably, a transmission dynamics model has been developed for cashew trees, focusing on disease transmission and stability analysis [16]. Another model examining the interaction between tomato plants and powdery mildew employs a compartmental approach based on the Waggoner host-disease system, categorizing leaves into healthy, diseased, and defoliated compartments [17]. Additionally, broader reviews have explored the role of mathematical models in understanding plant disease epidemics [18]. In contrast to these existing studies [16-18], our work presents two novel mathematical models that not only capture the transmission dynamics of powdery mildew but also introduce effective biological control strategies as alternatives to chemical fungicides, thereby promoting environmentally sustainable disease management. This emphasis on non-chemical interventions addresses growing concerns about the adverse effects of pesticides on human health and ecosystems. Furthermore, our incorporation of an optimal control framework adds a practical dimension by helping decision-makers manage treatment costs while maximizing disease suppression. By integrating biological realism with economic considerations, our models offer a more holistic and applicable approach to managing powdery mildew in agricultural systems.

This paper presents two mathematical models designed to address the challenges of powdery mildew disease in mango plants and fruits. The first model focuses on biological control strategies for managing the disease in mango plants, while the second examines the fungal dynamics of powdery mildew in mango fruits. Both models are extended to include optimal control measures, enabling the evaluation of the effectiveness and cost-efficiency of various treatment strategies. The contributions made by the authors Jin Wang and Alfred Hugo has always been a source of inspiration for this work [19-20]. The authors of the work [21-32] have contributed a lot in the experimental, analysis and review based studies in mango plant, which has been very efficient. Approximate analytical solutions are derived for these models using the New Homotopy Perturbation Method, Adomian Decomposition Method, and Variational Iteration Method. The accuracy of these solutions is validated by comparison with numerical solutions, with findings illustrated through graphical analyses and error tables. The strengths of this paper lie in its thorough approach to tackling powdery mildew disease using mathematical modeling. By creating models that incorporate both biological control and optimal control strategies, the study offers a comprehensive framework for disease management. Employing multiple analytical methods to derive approximate solutions adds to the reliability and robustness of the findings. Validation through numerical solutions further reinforces the credibility of the proposed models. Additionally, the inclusion of cost-effectiveness analysis provides valuable practical insights for decision-makers in the agricultural sector.

The paper is organized as follows: *Materials and Methods* section presents the formulation of the mathematical model, including system dynamics and assumptions. It also outlines the derivation of approximate analytical solutions using the New Homotopy Perturbation Method, Adomian Decomposition Method, and Variational Iteration Method and the construction of an optimal control strategy. The *Results and Discussions* section provides a detailed analysis of model's behavior through graphical simulations, highlighting the influence of key parameters on the dynamics of healthy, infected and controlled populations. The *Conclusion* section summarizes the main findings of the study, discusses potential applications, and offers directions for future research. The manuscript concludes with a complete list of references that support the theoretical and empirical foundations of this work.

2. MATHEMATICAL MODEL FORMULATION

2.1 Mathematical Model for Biological Control of Powdery Mildew Disease in Mango Plant (Model I)

The biological control model is developed to control the powdery mildew disease in Mango plants. Rather than chemical pesticides and fungicides, the biological way of controlling a disease is eco-friendly and harmless when a living being consumes it. This model is categorized into four compartments healthy H and infected mango plants I, pathogen *Oidium mangifera* population P, and biological control agent *Ampelomyces quisqualis* population B. The growth and the death rates of healthy mango plants, pathogen, and biological control agent population are given to be $\alpha, \alpha_P, \alpha_B$ and $\gamma_1, \gamma_2, \gamma_3$. The way *Ampelomyces quisqualis* helps in reducing *Oidium mangiferae* can be estimated using the parameter π. The mango host plants that die of powdery mildew disease can be monitored with the help of this parameter δ. The schematic representation of the model and the other list of parameters involved in this model are given in Figure 1 and Table 1.

$$\frac{dH}{dt} = \alpha - \beta HP - \gamma_1 H \tag{1}$$

$$\frac{dI}{dt} = \beta HP - \delta I - \theta I \tag{2}$$

$$\frac{dP}{dt} = \alpha_P P\left(1 - \frac{P}{K_1}\right) - \pi BP - \gamma_2 P \tag{3}$$

$$\frac{dB}{dt} = \alpha_B B\left(1 - \frac{B}{K_2}\right) - \gamma_3 B \tag{4}$$

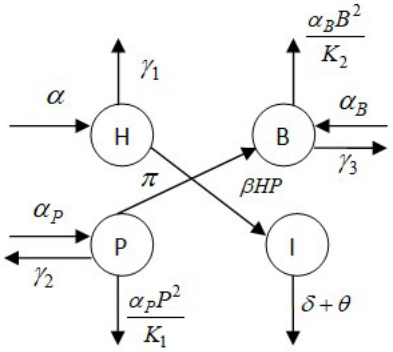

Figure 1. Schematic representation of biological control of powdery mildew disease (Model I).

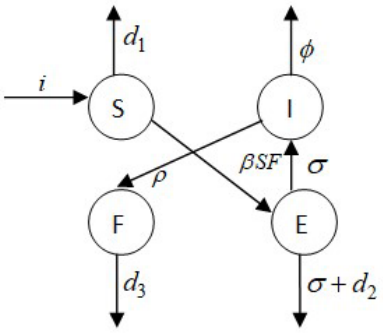

Figure 2. Schematic representation of fungal dynamics in mango fruit (Model II).

Table 1. List of parameters (Model I).

Symbol	Description	Baseline Value/Range	Source
α	The birth rate of healthy hosts	0.4-0.5 cm/day	[21]
α_P	The growth rate of the pathogen	0.0002-0.01cm/day	[22]
α_B	The growth rate of the biological control agent related to the pathogen population	0.001-0.3 cm/day	[23]
β	Infection rate coefficient	0.12-0.2/day	[24]
$\gamma_1, \gamma_2, \gamma_3$	Natural death rate of healthy hosts, pathogen and biological control agent	0.001-0.2/day	Assumed
δ	The recovery rate of infected hosts	0.01-1/day	[25]
θ	Disease-induced mortality rate of infected hosts	0.01-0.6/day	[26]
π	Effectiveness of the biological control agent in reducing the pathogen population	0.1-0.98/day	[27]
K_1, K_2	Carrying capacity of the pathogen and biological control agent population	1-2 individuals/m^3	Assumed

2.2 Mathematical Model for Analyzing Fungal Dynamics of Powdery Mildew Disease in Mango Fruit (Model II)

Powdery mildew disease also affects mango fruit in larger quantities, and it leads to yield loss. To observe the fungi behavior in mango fruit, a classical SEIF model is created. This model comprises four categories susceptible S, exposed E, and infected mango fruits I to understand the fungal dynamics, the rate of the *Oidium mangiferae* population F is formulated. The behavior of this fungi can be analyzed with the help of rate of infection from spores to susceptible fruits β, Rate of spore production from infected fruits ρ and Rate at which exposed fruits turn into infected fruits σ. The remaining parameter's description is given in Table 2 and the schematic representation of powdery mildew disease in mango fruit is given in Figure 2.

$$\frac{dS}{dt} = i - \beta SF - d_1 S \tag{5}$$

$$\frac{dE}{dt} = \beta SF - \sigma E - d_2 E \tag{6}$$

$$\frac{dI}{dt} = \sigma E - \phi I \tag{7}$$

$$\frac{dF}{dt} = \rho I - d_3 F \tag{8}$$

Table 2. List of parameters (Model II).

Symbol	Description	Baseline Value/Range	Source
i	Natural fruit production rate	0.03/annum	[28]
β	Rate of infection from spores to susceptible fruits	0.2-0.4	[29]
d_1, d_2, d_3	The natural decay rate of susceptible & exposed fruits and fungal spores	0.001-0.7	Assumed
σ	The rate at which exposed fruits turn into infected fruits	0.01-0.05	[29-30]
ϕ	Abscission rate or death rate of infected fruits	0.1-0.8	[31]
ρ	Rate of spore production from infected fruits	0.01-0.1/day	[32]

3. METHODOLOGY

This section presents the approximate analytical expressions for both models of powdery mildew disease in mango plants.

3.1 New Homotopy Perturbation Method (NHPM)

The New Homotopy Perturbation Method (NHPM) is an advanced version of the classical Homotopy Perturbation Method, which was developed by Ji-Huan He in the late 1990s. The classical HPM integrates the concept of homotopy from topology with perturbation techniques to solve non-linear differential equations. NHPM builds on this foundation by incorporating modifications that improve convergence and adaptability, making it especially effective for complex systems [33-34]. The step-by-step procedure is displayed in the Appendix section. The approximate analytical expressions for biological control and fungal dynamics of powdery mildew disease in mango plants and fruit (Model I, Model II) are obtained as,

$$H = \frac{\alpha}{\beta P(0)+\gamma_1} + \left(H_i - \frac{\alpha}{\beta P(0)+\gamma_1}\right) e^{-(\beta P(0)+\gamma_1)t} \tag{9}$$

$$I = \frac{\beta H(0)P(0)}{\delta+\theta} + \left(I_i - \frac{\beta H(0)P(0)}{\delta+\theta}\right) e^{-(\delta+\theta)t} \tag{10}$$

$$P = \frac{\alpha_P P(0)^2}{K_1(\alpha_P - \pi B(0) - \gamma_2)} + \left(P_i - \frac{\alpha_P P(0)^2}{K_1(\alpha_P - \pi B(0) - \gamma_2)}\right) e^{(\alpha_P - \pi B(0) - \gamma_2)t} \tag{11}$$

$$B = \frac{\alpha_B B(0)^2}{K_2(\alpha_B - \gamma_3)} + \left(B_i - \frac{\alpha_B B(0)^2}{K_2(\alpha_B - \gamma_3)}\right) e^{(\alpha_B - \gamma_3)t} \tag{12}$$

Also, the approximate analytical expression for model II is given by,

$$S = \frac{i}{\beta F(0)+d_1} + \left(S_i - \frac{i}{\beta F(0)+d_1}\right) e^{-(\beta F(0)+d_1)t} \tag{13}$$

$$E = \frac{\beta S(0)F(0)}{(\sigma+d_2)} + \left(E_i - \frac{\beta S(0)F(0)}{(\sigma+d_2)}\right) e^{-(\sigma+d_2)t} \tag{14}$$

$$I = \frac{\sigma E(0)}{\phi} + \left(I_i - \frac{\sigma E(0)}{\phi}\right) e^{-\phi t} \tag{15}$$

$$F = \frac{\rho I(0)}{d_3} + \left(F_i - \frac{\rho I(0)}{d_3}\right) e^{-d_3 t} \tag{16}$$

3.2 Adomian Decomposition Method (ADM)

The Adomian Decomposition Method, introduced by George Adomian in the 1980s, is a semi-analytical technique used to solve a broad range of linear and non-linear differential equations [35-36] We decompose the Equations (1-8), as linear, non-linear and remaining linear terms and assume the solution to be in the form of a power series.

$$H = H(0) + \alpha t - \beta(H(0)+\alpha t)P_0 t - \gamma_1(H(0)+\alpha t)t + \cdots \tag{17}$$

$$I = I(0) + \beta(H(0)+\alpha t)P_0 t - (\delta+\theta)I(0)t + \cdots \tag{18}$$

$$P = P(0) + \alpha_P P_0 t - \frac{\alpha_P P_0^2}{K_1} t - \pi B_0 P_0 t - \gamma_2 P_0 t + \cdots \tag{19}$$

$$B = B(0) + \alpha_B B_0 t - \frac{\alpha_B B_0^2}{K_2} t - \gamma_3 B_0 t + \cdots \tag{20}$$

In the same way for model II, we have,

$$S = S(0) + it - \beta(S(0)+it)F_0 t - d_1(S(0)+it)t + \cdots \tag{21}$$

$$E = E(0) + \beta(S(0)+it)F_0 t - (\sigma+d_2)E_0 t + \cdots \tag{22}$$

$$I = I(0) + (\sigma E_0 - \phi I_0)t + \cdots \tag{23}$$

$$F = F(0) + (\rho I_0 - d_3 F_0)t + \cdots \tag{24}$$

3.3 Variational Iteration Method (VIM)

The Variational Iteration Method was developed by Ji-Huan He in the 1990s. In this method, we carry out the iteration by constructing the correctional function [37-39]. Using this technique the approximate analytical expressions for both models are given as,

$$H_1(t) = H_0 + (\alpha - \beta H_0 P_0 - \gamma_1 H_0)t \tag{25}$$

$$I_1(t) = I_0 + (\beta H_0 P_0 - \delta I_0 - \theta I_0)t \tag{26}$$

$$P_1(t) = P_0 + \left(\left(\alpha_P P_0\left(1 - \frac{P_0}{K_1}\right)\right) - \pi B_0 P_0 - \gamma_2 P_0\right)t \tag{27}$$

$$B_1(t) = B_0 + \left(\left(\alpha_B B_0\left(1 - \frac{B_0}{K_2}\right)\right) - \gamma_3 B_0\right)t \tag{28}$$

Similarly, for model II we have,

$$S_1(t) = S_0 + (i - \beta S_0 F_0 - d_1 S_0)t \tag{29}$$

$$E_1(t) = E_0 + (\beta S_0 F_0 - \sigma E_0 - d_2 E_0)t \tag{30}$$

$$I_1(t) = I_0 + (\sigma E_0 - \phi I_0)t \quad (31)$$
$$F_1(t) = F_0 + (\rho I_0 - d_3 F_0)t \quad (32)$$

These approximate analytical expressions in Equations (17-32) are evaluated against the exact solution and the results are presented in the form of a graph. Wherever there is a deviation from the numerical solution, the error percentage is computed and presented in error in Tables 3 and 4. From Tables 3 and 4, based on the error percentages for each parameter, we can observe that the New Homotopy Perturbation Method is more efficient for both models I and II than the Adomian Decomposition Method and Variational Iteration Method as it converges to the numerical solution more or less accurately.

Table 3. Error percentage for Model I at time $t = 1$.

Parameter	Numerical	Analytical					
		NHPM	Error (%)	ADM	Error (%)	VIM	Error (%)
$\gamma_1(H)$	**0.4595**	**0.4595**	0	0.4366	4.98	0.4485	2.39
$\delta(I)$	**0.3787**	**0.3782**	0.13	0.3782	0.13	0.3775	0.32
$\alpha_P(P)$	**0.2903**	**0.2896**	0.24	0.2898	0.17	0.2895	0.28
$\gamma_3(B)$	**0.1723**	**0.1724**	0	0.1724	0.06	0.1702	1.22
Average error (%)			0.0925		1.3350		1.0525

Table 4. Error percentage for Model II at time $t = 1$.

Parameter	Numerical	Analytical					
		NHPM	Error (%)	ADM	Error (%)	VIM	Error (%)
$d_1(S)$	**0.4767**	**0.4747**	0.42	0.4752	0.31	0.4582	3.88
$\phi(I)$	**0.3179**	**0.3179**	0	0.3180	0.03	0.3050	4.06
$d_3(F)$	**0.3012**	**0.3013**	0.03	0.3012	0	0.3013	0.03
Average error (%)			0.1500		0.1133		2.6567

4. OPTIMAL CONTROL

The objective of constructing the optimal control model is to reduce the spread of the disease and to minimize the cost associated with treatments [20, 40-41]. The optimal control model for powdery mildew disease of mango fruit is constructed as follows,

$$\frac{dS}{dt} = i - (1-u_1)\beta SF - d_1 S \quad (33)$$
$$\frac{dE}{dt} = (1-u_1)\beta SF - (\sigma - u_2)E - d_2 E \quad (34)$$
$$\frac{dI}{dt} = (\sigma - u_2)E - \phi I \quad (35)$$
$$\frac{dF}{dt} = (\rho - u_3)I - d_3 F \quad (36)$$

where u_1, u_2, u_3 are control variables like the application of antifungal agents to inhibit germination of spores, post-harvest treatment like hot water dip or ultra-violet (UV) light that can reduce the progression of infection and rate of introducing microbial antagonists (ex., Bacillus or Trichoderma spp) to reduce the spore production on infected fruits. The total objective function is of the form,

$$J = \min_{u_1,u_2,u_3} \int_0^{t_f} \left(A_1 I + A_2 F + \frac{1}{2}B_1 u_1^2 + \frac{1}{2}B_2 u_2^2 + \frac{1}{2}B_3 u_3^2 \right) dt \quad (37)$$

where $A_1 I, A_2 F$ indicates the weight associated with reducing the infected mango and fungi population and B_1, B_2, B_3 indicates the relative cost for each control measure like the antifungal, post-harvest, and microbial treatment for the fungi removal. By Pontryagin's Maximum Principle [42], the adjoint variables $\lambda_1, \lambda_2, \lambda_3, \lambda_4$ are introduced to capture the sensitivity of the objective function concerning changes in state variables S, E, I, F. Thus the Hamiltonian function (H) is constructed as,

$$H = A_1 I + A_2 F + \frac{1}{2} B_1 u_1^2 + \frac{1}{2} B_2 u_2^2 + \frac{1}{2} B_3 u_3^2 + \lambda_1 (i - (1 - u_1)\beta SF - d_1 S) + \lambda_2 \big((1 - u_1)\beta SF - (\sigma - u_2)E - d_2 E\big) + \lambda_3 \big((\sigma - u_2)E - \phi I\big) + \lambda_4 (\rho - u_3) I - d_3 F$$

Then the adjoint equations are obtained by, $\frac{\partial \lambda_i}{\partial t} = -\frac{\partial H}{\partial i}$, with transversality boundary condition $\lambda_i(t_f) = 0$. Thus, the adjoint equations for this optimal control model are given to be,

$$\frac{\partial H}{\partial S} = -\lambda_1(-(1 - u_1)\beta F - d_1) - \lambda_2(1 - u_1)\beta F \tag{38}$$

$$\frac{\partial H}{\partial E} = -\lambda_2(-(\sigma - u_2) - d_2) - \lambda_3(\sigma - u_2) \tag{39}$$

$$\frac{\partial H}{\partial I} = -A_1 + \lambda_3 \phi - \lambda_4(\rho - u_3) \tag{40}$$

$$\frac{\partial H}{\partial F} = -A_2 + \lambda_4 d_3 - \lambda_1(-(1 - u_1)\beta S) - \lambda_2(1 - u_1)\beta S \tag{41}$$

The optimality of the control problem is obtained by,

$$u_i^*(t) = \frac{\partial H}{\partial u_i} \tag{42}$$

$$\frac{\partial H}{\partial u_1} = B_1 u_1 + \beta SF\lambda_1 - \beta SF\lambda_2 \tag{43}$$

$$\frac{\partial H}{\partial u_2} = B_2 u_2 + \lambda_2 E - \lambda_3 E \tag{44}$$

$$\frac{\partial H}{\partial u_3} = B_3 u_3 - \lambda_4 I \tag{45}$$

Thus, the compact form of the solution $u_1^*(t), u_2^*(t), u_3^*(t)$ is given as follows,

$$u_1^*(t) = \min\left\{\max\left\{0, \frac{\beta SF(\lambda_2 - \lambda_1)}{B_1}\right\}, 1\right\} \tag{46}$$

$$u_2^*(t) = \min\left\{\max\left\{0, \frac{E(\lambda_3 - \lambda_2)}{B_2}\right\}, 1\right\} \tag{47}$$

$$u_3^*(t) = \min\left\{\max\left\{0, \frac{\lambda_4 I}{B_3}\right\}, 1\right\} \tag{48}$$

The optimal control model in Equations (33-36) and model II in Equations (5-8) are plotted and the results are presented in the form of a graph from Figures 3-6. Figures 3 and 4 show that optimal control measures, such as the application of antifungal agents to inhibit the germination of spores u_1, post-harvest treatment like hot water dip or UV light that can reduce the progression of infection u_2, lead to an increase in susceptible and exposed mango fruits over time. These interventions effectively reduce the infection rate, allowing more fruits to remain in the susceptible or exposed stages without advancing to the infected stage. From Figures 5 and 6 we can see that, as the objective function is formulated to minimize the infected mango fruit and fungal population, we have attained the desired result. The curve representing infected mango fruits under optimal control is significantly lower compared to the scenario without control. Under optimal control conditions like the rate of introducing microbial antagonists u_3, the fungal population is significantly reduced due to the disruption of the fungus's reproduction and spread. We have also presented data which shows the costs corresponding to the treatments in Table 5.

Although the proposed optimal control strategies provide a solid mathematical foundation for managing disease, their implementation in actual scenarios may face several obstacles. Field conditions often involve limited or imprecise real-time data on fungal infection levels and environmental factors. Additionally, timely execution of biological or chemical control methods may be hindered by constraints such as limited resources, labor shortages, or unpredictable weather. To address these challenges, future studies could focus on integrating the model with precision agriculture technologies, including automated disease detection systems, weather-based alerts, and adaptive control mechanisms capable of real-time responses. Engaging with agricultural practitioners and factoring in cost-effectiveness during the design of control strategies could further improve the model's practical viability.

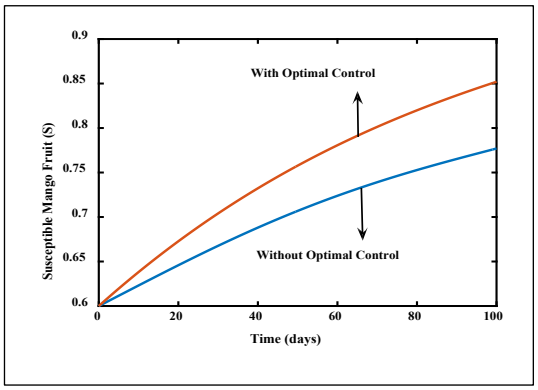

Figure 3. Susceptible mango vs time.

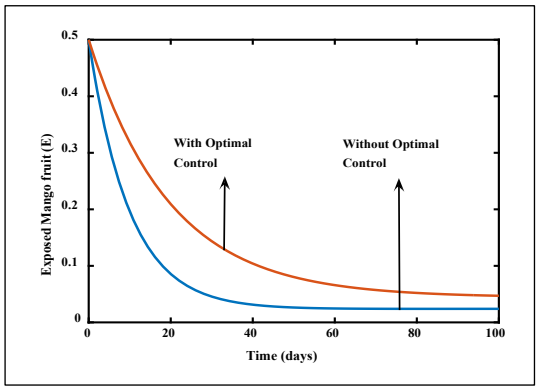

Figure 4. Exposed mango vs time.

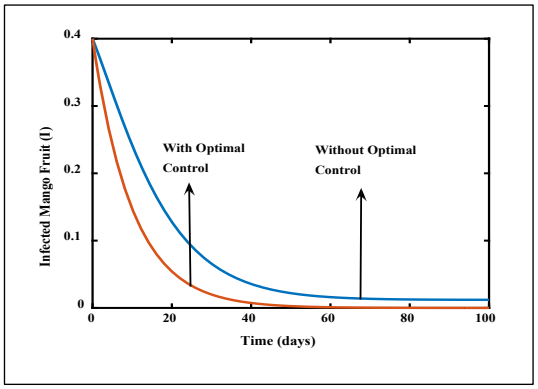

Figure 5. Infected mango vs time.

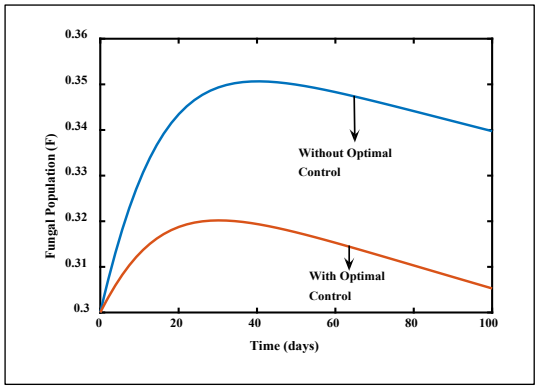

Figure 6. Fungal population vs time.

Table 5. Costs associated with each control measure and used for simulations.

Symbols	Description	Value
A_1	Weight associated with reducing infected mango plant	1
A_2	Weight associated with reducing the fungal population	1
B_1	Weight on the cost of antifungal agents to inhibit germination of spores	0.9
B_2	Weight on the cost of post-harvest treatment like hot water dip or UV light	0.9
B_3	Weight on the cost of microbial antagonists (ex., Bacillus or Trichoderma spp) to reduce the spore production	0.9

5. RESULTS AND DISCUSSIONS

In this section, we will discuss in detail the behavior of the parameters for each system. The approximate analytical expressions for Model I and Model II are derived using the New Homotopy Perturbation Method (Equations (9-16)), Adomian Decomposition Method (Equations (17-24)) and Variational Iteration Method (Equations (25-32)) and verified for its accuracy against the numerical solution using MATLAB's ode45 function. The results are presented in the form of a graph. In every graph, the blue solid line represents the numerical solution, and the dashed line, star, square markers represent the analytical solution of NHPM, ADM, and VIM methods.

Figures 7 to 10 represent the behavior representation of parameters in Equations (1-4). A higher growth rate α implies that the mango plants are proliferating at a faster rate which is evident in Figure 7(a), offsetting any losses from infections or natural death. From Figure 7(b) we see that the infection rate coefficient β, which controls the transition of healthy mango plants to infected states, has a significant negative impact on the population of healthy plants; for higher values of the infection rate coefficient, the rate at which healthy plants become infected accelerates, resulting in a rapid decline in the healthy mango population $H(t)$. High natural mortality γ_1 lowers the capacity of the healthy plant population as shown in Figure 7(c) to sustain itself, exacerbating the effects of infection and making the decline in healthy hosts more severe. Over time, the number of infected mango plants $I(t)$ is directly and significantly impacted by the infection rate coefficient parameter β. The population of diseased plants grows in tandem with the rate at which healthy plants become infected, which increases as this parameter rises and is displayed in Figure 8(a). The population of diseased plants is suppressed by the recovery rate parameter δ, which shows how quickly infected plants recover and return to a healthy state. The recovery rate (δ), depicted in Figure 8(b), has the opposite effect, higher δ values result in a gradual decline in the infected population. Figure 8(c) highlights the role of the disease-induced mortality rate (θ); increasing θ accelerates the removal of infected individuals, leading to a more rapid decrease in $I(t)$.

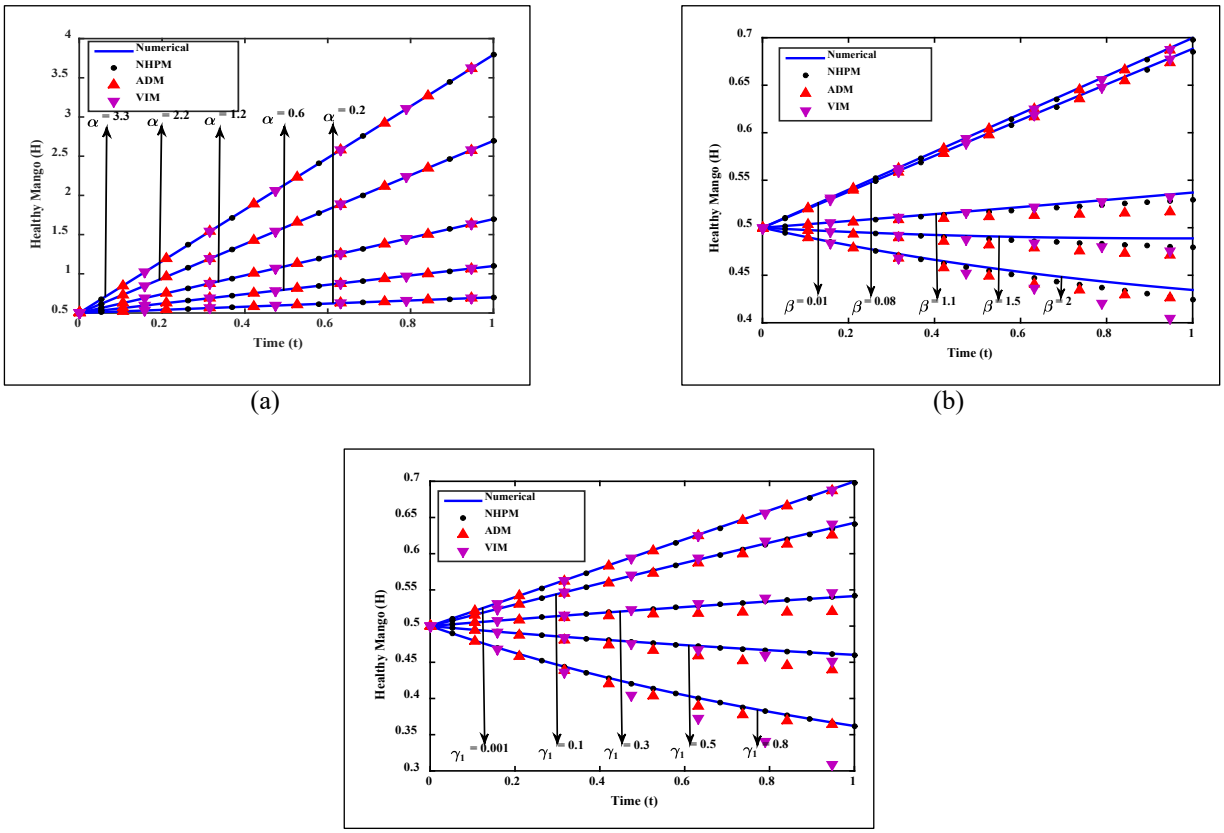

(a) (b) (c)

Figure 7. The rate of healthy mango with respect to the parameters (a) Birth rate of healthy hosts α, (b) Infection rate coefficient β, (c) Natural death rate of healthy hosts γ_1.

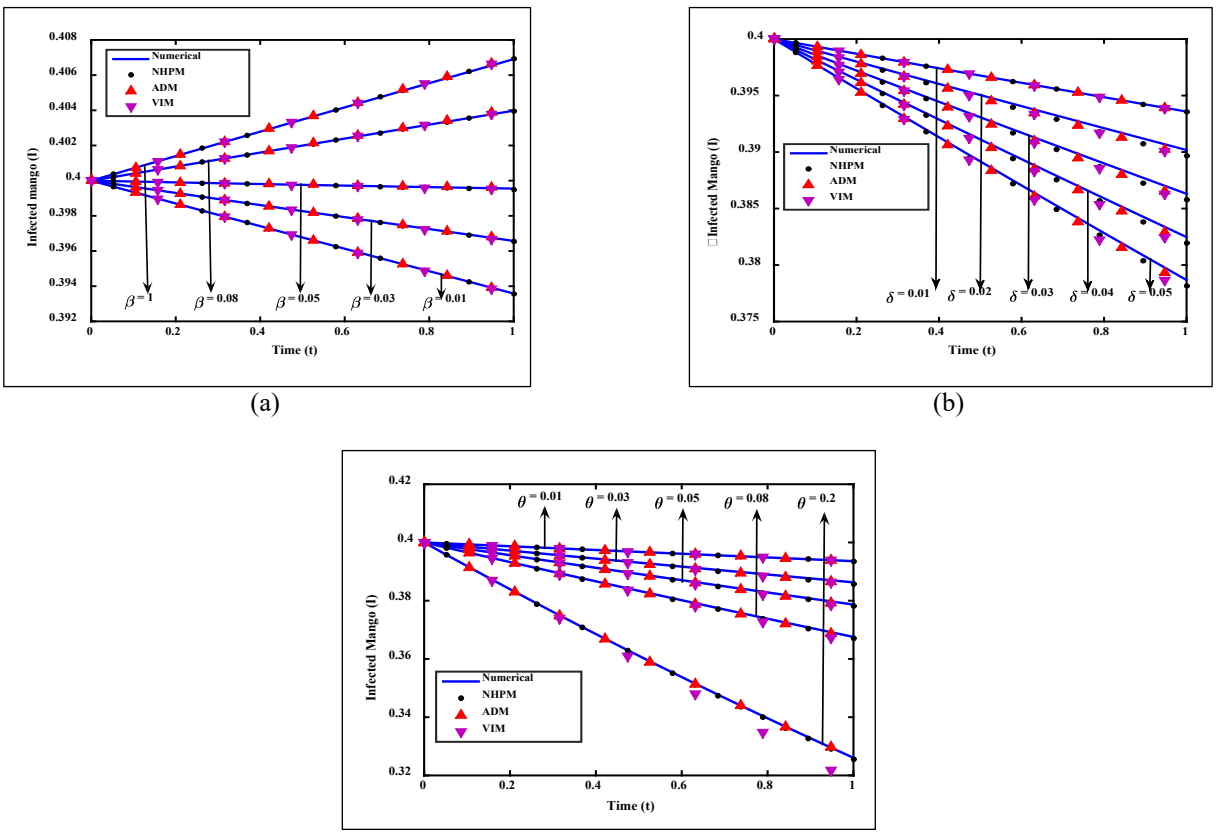

(a) (b) (c)

Figure 8. The rate of infected mangoes concerning the parameters (a) Infection rate coefficient β, (b) Recovery rate of infected hosts δ, (c) Disease induced mortality rate of infected hosts θ.

Surprisingly, in Figure 9(a) when the pathogen's intrinsic growth rate α_P increases, the pathogen population $P(t)$ gradually declines. This points to a feedback mechanism in which the pathogen's quick spread exhausts resources (such as vulnerable hosts or environmental nutrients), ultimately reducing its own growth and resulting in a decline. A decrease in the pathogen population over time observed in Figure 9(b) is closely correlated with an increase in the biological control agents' ability π to reduce the pathogen population. Similarly, increasing the natural mortality rate (γ_2) reduces the pathogen population more sharply, as demonstrated in Figure 9(c). Figure 10(a) indicates that as the biological control agent's growth rate α_B increases, its population increases over time. The figures demonstrate a positive relationship between the growth rate parameter and population size, with higher growth rates leading to faster and more significant increases in the biological control agent population $B(t)$. In contrast, Figure 10(b) shows that increasing the natural death rate (γ_3) leads to a pronounced decline in their population, underscoring the sensitivity of biological control sustainability to mortality factors.

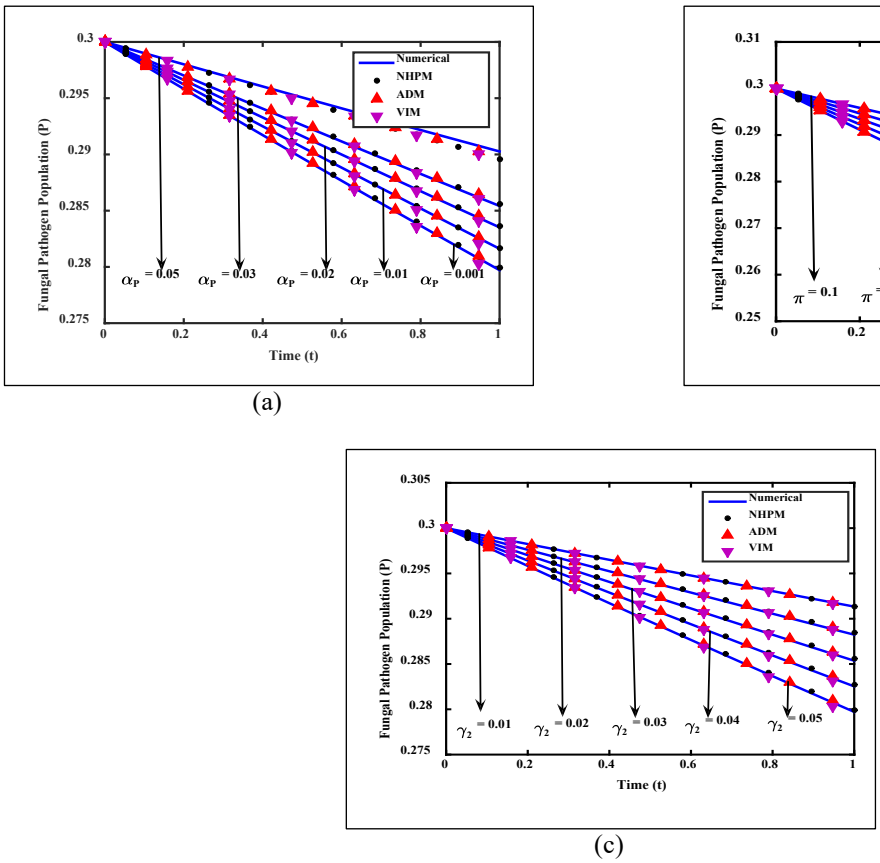

(a) (b) (c)

Figure 9. The rate of fungal pathogen *Oidium mangiferae* population concerning the parameters (a) Growth rate of the pathogen α_P, (b) Effectiveness of the biological control agent in reducing the pathogen population π, (c) Natural death rate of pathogen γ_2.

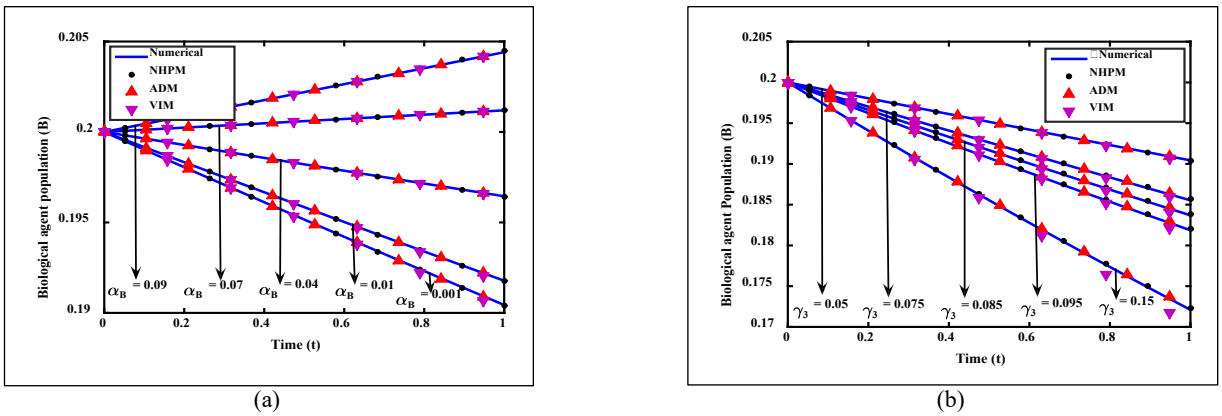

(a) (b)

Figure 10. The rate of biological control agent *Ampelomyces quisqualis* population concerning the parameters (a) Growth rate of the biological control agent α_B, (b) Natural death rate of biological control agent γ_3.

Figures 11 to 13 represents the behavior representation of parameters in system (2). The susceptible mango fruit population $S(t)$ grows as the natural fruit production rate parameter i increases which can be noted in Figure 11(a). The figures show that higher production rates result in a larger pool of susceptible fruits over time, indicating a robust replenishment mechanism. However, as shown in Figure 11(b), increasing the infection rate (β) reduces $S(t)$ due to more fruits transitioning to the infected class. Likewise, Figure 11(c) reveals that higher decay rates (d_1) lead to a quicker decline in susceptible fruits, representing intrinsic deterioration or damage. The death rate of infected fruits represents the rate at which infected fruits are removed from the population due to factors such as disease-induced degradation, natural senescence, or external interventions (e.g., manual removal of infected fruits). The infected fruit population $I(t)$ declines with increasing death rates (ϕ), as seen in Figure 12(a), reflecting removal due to disease or external factors. Figure 12(b) shows that the transition rate from exposed to infected fruits (σ) determines how rapidly fruits become actively infected; higher values of σ lead to quicker disease progression. One important source term in the differential equation that models the fungal population is the rate at which spores are produced from infected fruits. The rate of spore generation ρ is directly correlated with fungal population $F(t)$. A net increase in the size of the fungus population is seen in Figure 13(a) which results in acceleration of the influx of new spores into the population as the parameter value rises. The fungal population's differential equation includes a loss factor that is influenced by the spores' inherent rate of decay d_3. Figure 13(b) shows that the spore decay rate (d_3) reduces $F(t)$, although fungi may counterbalance this through increased production and germination. The analytical results align closely with numerical simulations, validating the model. Any deviations were quantified through error percentage comparisons between analytical approximations and numerical results, as shown in Tables 3 and 4.

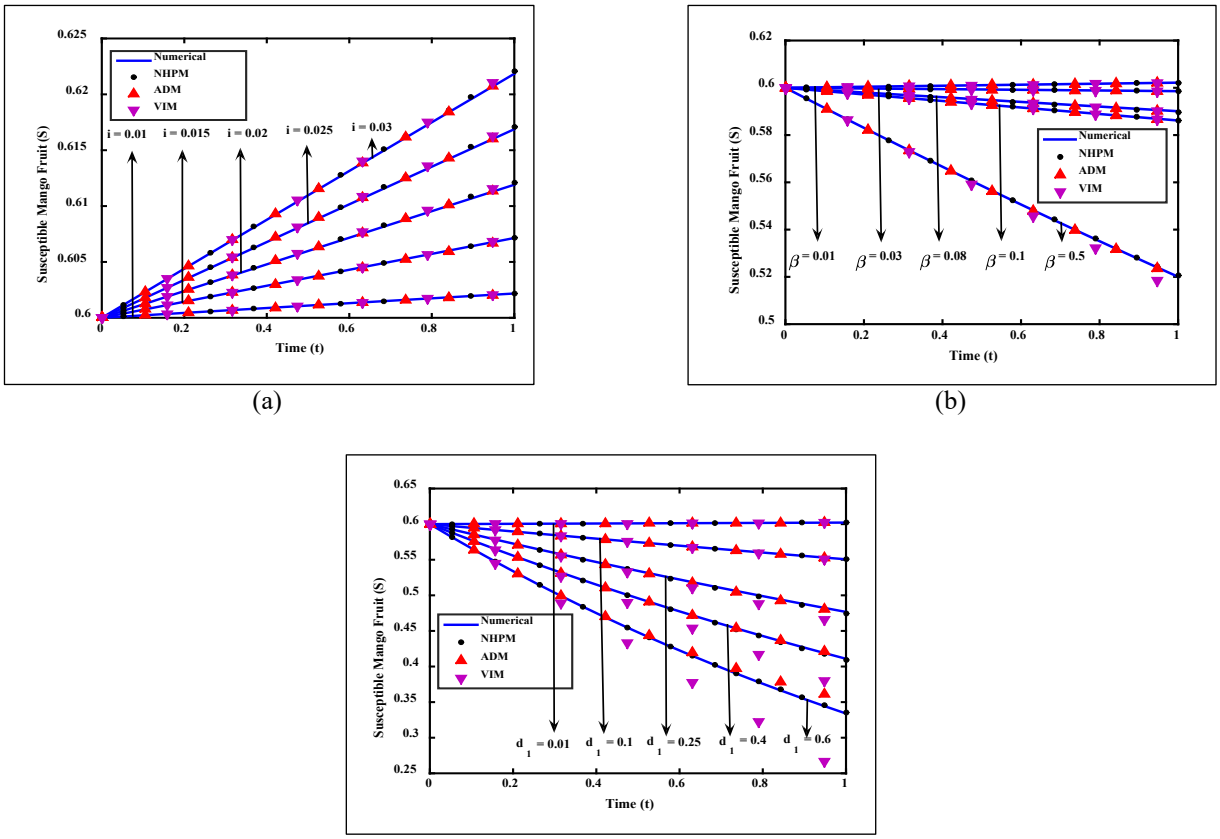

Figure 11. The rate of susceptible mango fruit concerning the parameters (a) Natural fruit production rate i, (b) Rate of infection from spores to susceptible fruits β, (c) Natural decay rate of susceptible fruits d_1.

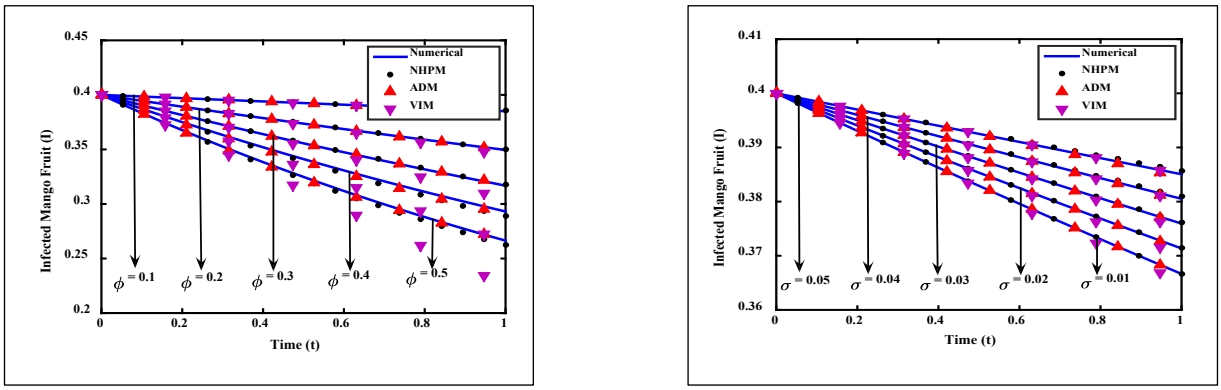

(a) (b)

Figure 12. The rate of infected mango fruit concerning the parameters (a) Abscission rate or death rate of infected fruits ϕ, (b) Rate at which exposed fruits turn into infected fruits σ.

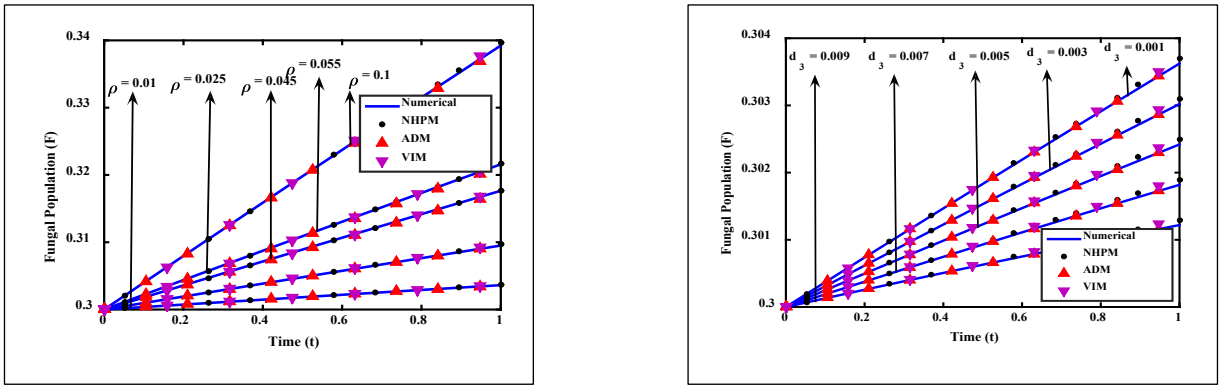

(a) (b)

Figure 13. The rate of fungal pathogen *Oidium mangiferae* population concerning the parameters (a) Rate of spore production from infected fruits ρ, (b) Natural decay rate of fungal spores d_3.

This study presumes constant parameter values throughout the temporal domain, thereby streamlining the analytical framework. However, such an assumption may not adequately capture the complexity of real-world dynamics. In reality, variables such as the proliferation rate of fungi, transmission intensity, and the success of bio-control measures are subject to fluctuation due to external factors including ambient temperature, atmospheric moisture, and periodic environmental changes. Future studies could benefit from exploring formulations that incorporate temporally adaptive parameters or environmentally driven functions to better reflect these evolving mechanisms. The integration of observed climatic datasets or the linkage of the model to agro-meteorological platforms may substantially improve forecasting capability and broaden its utility across diverse ecological contexts.

6. CONCLUSION

This study has developed mathematical models to understand fungal dynamics in mango fruits and manage powdery mildew in mango trees. By incorporating optimal control strategies, the optimal value for the control variable parameters u_1, u_2, u_3 have been derived which is efficient in disease control and cost reduction. New Homotopy Perturbation Method, Adomian Decomposition Method, and Variational Iteration Method yielded accurate analytical solutions which are validated against numerical solutions. Error and graphical analyses confirm the models' reliability and precision. The average error percentage indicates that the New Homotopy Perturbation Method is more efficient than other analytical techniques. Combining biological insights with mathematical methods, this work provides practical solutions for a pressing agricultural challenge. Future research could expand upon this study by integrating more complex environmental and ecological factors into the models, such as climate variability, host genetic diversity, and interspecies interactions. Field trials to experimentally validate the proposed models would further demonstrate their practical applicability.

ACKNOWLEDGMENT AND FUNDING

The authors would like to thank the Principal and the Head of the Department of the institution for their constant support towards the research work. This work has not received any funds or grants from any organization.

DECLARATION O F CONFLICTING INTERESTS

The authors declare no potential conflicts of interest with respect to the research and publication of this article.

REFERENCES

[1] M. Nasir, S. M. Mughal, T. Mukhtar and M. Z. Awan, Powdery mildew of mango: A review of ecology, biology, epidemiology and management, *Crop Protection*, 64, 2014, 19-26.

[2] R. Felix-Gastelum, G. Herrera Rodriguez, C. Martinez Valenzuela, R. Longoria Espinoza, I. Maldonado Mendoza, F. Quiroz Figueroa, J. Martinez Alvarez, L. Garcia Perez and S. Espinosa Matias, First report of powdery mildew (pseudoidium anacardii) of mango trees in Sinaloa, Mexico, *Plant Disease*, 97(7), 2013.

[3] M. Reuveni, L. Gur and A. Farber, Development of improved disease management for powdery mildew on mango trees in Israel, *Crop Protection*, 110, 2018, 221-228.

[4] M. M. E. Abo Rehab, N. A. Shenoudy and H. M. Anwar, Effect of powdery mildew on mango chlorophyll content and disease control, *Egyptian Journal of Agricultural Research*, 92(2), 2014, 451-464.

[5] M. Reuveni, M. Harpaz and R. Reuveni, Integrated control of powdery mildew on field-grown mango trees by foliar sprays of mono-potassium phosphate fertilizer, sterol inhibitor fungicides and the strobilurin kresoxym-methyl, *European Journal of Plant Pathology*, 104(9), 1998, 853-860.

[6] Shahid Iqbal, Muhammad Atiq, Muhammad Fayyaz, Muhammad Zakria, Nasir Ahmed Rajput, Aasma, Ghalib Ayaz Kachelo, Ijaz Ahmad, Muhammad Usman and Asim Mehmood, Powdery mildew of mango: current status, perspective and emerging tools for management, *Agricultural Sciences Journal*, 6(1), 2024, 92-101.

[7] S. Hasan Naqvi, R. Perveen, S. Manzoor, H. Imran Umar, M. Iqbal, F. Liaquat, T. Majid and A. Irshad, Evaluation of various mango varieties against the infection dynamics of powdery mildew (Oidiummangiferae), *American Journal of Plant Sciences*, 5(15), 2014, 2372-2377.

[8] S. Kumar and B. Gupta, Hybrid CNN-random forest framework for elevated accuracy in powdery mildew disease classification, *3rd International Conference for Innovation in Technology (INOCON)*, 2024, 1-6.

[9] S. Kulkarni, T. Chavan and K. N. Vijaykumar, Management of Mango powdery mildew through potential organic products, *International Journal of Bio-resource and Stress Management*, 14, 2023, 756-761.

[10] R. R. Nalawade, S. D. Sawant, M. S. Joshi, P. M. Ingle, V. G. More and J. J. Kadam, Mango Anthracnose and powdery mildew disease detection using convolutional neural network and artificial neural network, *Journal of Plant Disease Sciences*, 18(1), 2023, 11-19.

[11] M. Ahmed, S. Khalifa and E. El-Bassel, Evaluation of some biocontrol agents to control mango powdery mildew disease and their effect on productivity, *Journal of Plant Protection and Pathology*, 14(1), 2023, 13-19.

[12] L. Gong, C. Yu, K. Lin and C. Liu, A lightweight powdery mildew disease evaluation model for its in-field detection with portable instrumentation, *Agronomy*, 12(1), 2021, 97.

[13] J. Zhao, Y. Fang, G. Chu, H. Yan, L. Hu and L. Huang, Identification of leaf-scale wheat powdery mildew (Blumeria graminis f. sp. Tritici) combining hyperspectral imaging and an SVM classifier, *Plants*, 9(8), 2020, 936.

[14] X. Chang, M. Huang, A. Guo, W. Huang, Z. Cai, Y. Dong, J. Guo, Z. Hao, Y. Huang, K. Ren, B. Hu, G. Chen, H. Su, L. Li and Y. Liu, Early detection of rubber tree powdery mildew by combining spectral and physicochemical parameter features, *Remote Sensing*, 16(9), 2024, 1634.

[15] A. Muthu Kumar, J. Cruz Antony and V. Soundararajan, Classification of powdery mildew disease symptoms on sandalwood using machine learning techniques, *European Journal of Forest Engineering*, 10(2), 2024, 84-91.

[16] F. M. Mrope, N. Nyerere and F. A. Mgandu, Modeling the transmission dynamics of powdery mildew disease in cashew plants, *Modeling Earth Systems and Environment*, 11(3), 2025, 182.

[17] J. Chelal and B. Hau, Modelling the interaction between powdery mildew epidemics and host dynamics of tomato, *European Journal of Plant Pathology*, 2015, 461-479.

[18] N. Bazarra, M. Colturato, J. R. Fernandez, M. G. Naso, A. Simonetto and G. Gilioli, Analysis of a mathematical model arising in plant disease epidemiology, *Applied Mathematics & Optimization*, 85(2), 2022, 19.

[19] C. Yang and J. Wang, A mathematical model for frogeye leaf spot epidemics in soybean, *Mathematical Biosciences and Engineering*, 21(1), 2023, 1144-1166.

[20] A. Hugo, E. Lusekelo, and R. Kitengeso, Optimal control and cost effectiveness analysis of tomato yellow leaf curl virus disease epidemic model tomato paper, *Applied Mathematics*, 9(3), 2019, 82-88.

[21] E. F. Gilman, D. G. Watson, R. W. Klein, A. K. Koeser, D. R. Hilbert and D. C. McLean, Mangifera indica: Mango, *IFAS* Extension, 1993.

[22] A. K. Misra, M. B. Dalvi, R. Agarwal and B. R. Salvi, Forewarning powdery mildew of mango (Mangifera indica L.) caused by oidium mangifereae berthet, *Journal of Eco-friendly Agriculture*, 12(1), 2017, 1-9.

[23] L. Kiss, A review of fungal antagonists of powdery mildews and their potentials as biocontrol agents, *Pest Management Science*, 59(4), 2003, 475-483.

[24] M. Kumar, V. Ponnuswami, S. Ramesh Kumar and V. Arumugam, Correlation between weather and yield attributes of mango, *Research in Environment and Life Sciences*, 7(3), 2014, 187-190.

[25] S. Diarra, S. Sory, M. O. Diawara, B. M. Traore and A. Sidibe, Cultivation practices of mango (Mangifera indica) varieties kent and keitt planters and the origins of orchard vulnerability to rainfall variability in the Koulikoro District, *International Journal of Agricultural Economics*, 6(4), 2021, 172-180.

[26] T. V. Galdino, S. Kumar, L. S. Oliveria, A. C. Alfenas, L. G. Neven, A. M. Al-Sadi and M. C. Picanco, Mapping global potential risk of mango sudden decline disease caused by ceratocystis fimbriata, *Plos One*, 11(7), 2016, e0159450.
[27] Y. Elad, B. Kirshner, N. Yehuda and A. Sztejnberg, Management of powdery mildew and gray mold of cucumber by Trichoderma harzianum T39 and Ampelomyces Quisqualis AQ10, *Bio Control*, 43(2), 1998, 241-251.
[28] S. P. Singh, L. K. Adarsha, A. K. Nandi and O. Jopir, Production performance of fresh mango in India: A growth and variability analysis, *International Journal of Pure and Applied Biosciences*, 6(2), 2018, 935-941.
[29] S. A. H. Naqvi, R. Perveen, S. A. Manzoor, H. M. I. Umar, M. T. Iqbal, F. Liaquat, T. Majid and A. Irshad, Evaluation of various mango varieties against the infection dynamics of powdery mildew (Oidium mangiferae Bert.), *American Journal of Plant Sciences*, 5(15), 2014.
[30] C. Nelson, *Mango Powdery Mildew*, Plant Disease, College of Tropical Agriculture and Human Resources, 2008.
[31] P. Gupta, *Powdery Mildew of Mango*, Dr. Kalam Agricultural College, Kishanganj, 2020.
[32] V. V. Patil, *Studies on Pathogens Associated with Fruit Drop of Mango* (*Mangifera Indica L.*), M.Sc. Thesis, Mahatma Phule Vidyapeeth, India, 2001.
[33] S. Rekha and L. Rajendran, Mathematical modeling of nonlinear vibrations of single-walled carbon nanotubes, Chapter 16, *Carbon Nanomaterials and Their Composites as Adsorbents,* Springer, 2024, 275-286.
[34] T. Roy and D. K. Maiti, An optimal and modified homotopy perturbation method for strongly nonlinear differential equations, *Nonlinear Dynamics*, 111(16), 2023, 15215-15231.
[35] R. O. Awonusika, Analytical solution of a class of Lane–Emden equations: Adomian decomposition method, *The Journal of Analysis*, 32(2), 2024, 1009-1056.
[36] M. Ramanathan and V. Kalirajan, Implementation of Adomian decomposition method for maize streak virus disease model to reduce the contamination rate in maize plant, *Mapana Journal of Sciences*, 22(2), 2023,56-78.
[37] J. H. He and X. H. Wu, Variational iteration method: New development and applications, *Computers & Mathematics with Applications*, 54(7), 2007, 881-894.
[38] S. Mungkasi, Variational iteration and successive approximation methods for a SIR epidemic model with constant vaccination strategy, *Applied Mathematical Modelling*, 90, 2021, 1-10.
[39] A. M. Wazwaz, Optical bright and dark soliton solutions for coupled nonlinear Schrodinger (CNLS) equations by the variational iteration method, *Optik*, 207, 2020, 1664457.
[40] W. Chukwu, F. Nyabadza and J. K. K. Asamoah, A mathematical model and optimal control for Listeriosis disease from ready-to-eat food products, *International Journal of Computing Science and Mathematics*, 17(1), 2023.
[41] T. K. Kar and S. Jana, A theoretical study on mathematical modelling of an infectious disease with application of optimal control, *Biosystems*, 111(1), 2013, 37-50.
[42] R. E. Kopp, Pontryagin maximum principle, *Mathematics in Science and Engineering*, 5, 1962, 255-279.

APPENDIX

Application of New Homotopy Perturbation Method

We construct the homotopy for the equation as follows,

$$(1-p)\left[\frac{dH}{dt}-\alpha+\beta HP(t=0)+\gamma_1 H\right]+p\left[\frac{dH}{dt}-\alpha+\beta HP+\gamma_1 H\right]=0 \tag{49}$$

$$(1-p)\left[\frac{dI}{dt}-\beta H(t=0)P(t=0)+\delta I+\theta I\right]+p\left[\frac{dI}{dt}-\beta HP+\delta I+\theta I\right]=0 \tag{50}$$

$$(1-p)\left[\frac{dP}{dt}-\alpha_P P+\frac{\alpha_P P^2(t=0)}{K_1}+\pi B(t=0)P\mp\gamma_2 P\right]+p\left[\frac{dP}{dt}-\alpha_P P\left(1-\frac{P}{K_1}\right)+\pi BP+\gamma_2 P\right]=0 \tag{51}$$

$$(1-p)\left[\frac{dB}{dt}-\alpha_B B+\frac{\alpha_B B^2(t=0)}{K_2}+\gamma_3 B\right]+p\left[\frac{dB}{dt}-\alpha_B B\left(1-\frac{B}{K_2}\right)+\gamma_3 B\right]=0 \tag{52}$$

$$(1-p)\left[\frac{dS}{dt}-i+\beta SF(t=0)+d_1 S\right]+p\left[\frac{dS}{dt}-i+\beta SF+d_1 S\right]=0 \tag{53}$$

$$(1-p)\left[\frac{dE}{dt}-\beta S(t=0)F(t=0)+\sigma E+d_2 E\right]+p\left[\frac{dE}{dt}-\beta SF+\sigma E+d_2 E\right]=0 \tag{54}$$

$$(1-p)\left[\frac{dI}{dt}-\sigma E(t=0)+\phi I\right]+p\left[\frac{dI}{dt}-\sigma E+\phi I\right]=0 \tag{55}$$

$$(1-p)\left[\frac{dF}{dt}-\rho I(t=0)+d_3 F\right]+p\left[\frac{dF}{dt}-\rho I+d_3 F\right]=0 \tag{56}$$

Then we replace each compartment in the form of a series as,

$$v=v_0+pv_1+p^2v_2+\cdots$$

Comparing the coefficients of like powers of p, we get,

$$p^0: \quad \frac{dH_0}{dt} - \alpha + \beta H_0 P(t=0) + \gamma_1 H_0 = 0 \tag{57}$$

$$\frac{dI_0}{dt} - \beta H(t=0)P(t=0) + \delta I_0 + \theta I_0 = 0 \tag{58}$$

$$\frac{dP_0}{dt} - \alpha_P P_0 + \frac{\alpha_P P^2(t=0)}{K_1} + \pi B(t=0)P_0 + \gamma_2 P_0 = 0 \tag{59}$$

$$\frac{dB_0}{dt} - \alpha_B B_0 + \frac{\alpha_B B^2(t=0)}{K_2} + \gamma_3 B_0 = 0 \tag{60}$$

$$\frac{dS_0}{dt} - i + \beta S_0 F(t=0) + d_1 S_0 = 0 \tag{61}$$

$$\frac{dE_0}{dt} - \beta S(t=0)F(t=0) + \sigma E_0 + d_2 E_0 = 0 \tag{62}$$

$$\frac{dI_0}{dt} - \sigma E(t=0) + \phi I_0 = 0 \tag{63}$$

$$\frac{dF_0}{dt} - \rho I(t=0) + d_3 F_0 = 0 \tag{64}$$

Then on integrating Equations (57-64), we arrive at the approximate analytical expression as given in Equations (9-16).

Application of Adomian Decomposition Method

On applying the differential and integration operator L and L^{-1} after decomposing the equation into linear, non-linear, remaining linear terms and assuming the solution to be in the form of a power series for Equations (9-16), we have,

$$\sum_{n=0}^{\infty} H_n = H(0) + L^{-1}(\alpha) - L^{-1}\left(\beta \sum_{n=0}^{\infty} A_n\right) - L^{-1}\left(\gamma_1 \sum_{n=0}^{\infty} H_n\right) \tag{65}$$

$$\sum_{n=0}^{\infty} I_n = I(0) + L^{-1}\left(\beta \sum_{n=0}^{\infty} A_n\right) - L^{-1}\left((\delta+\theta) \sum_{n=0}^{\infty} I_n\right) \tag{66}$$

$$\sum_{n=0}^{\infty} P_n = P(0) + L^{-1}\left(\alpha_P \sum_{n=0}^{\infty} P_n\right) - L^{-1}\left(\frac{\alpha_P}{K_1} \sum_{n=0}^{\infty} J_n\right) - L^{-1}\left(\pi \sum_{n=0}^{\infty} C_n\right) - L^{-1}\left(\gamma_2 \sum_{n=0}^{\infty} P_n\right) \tag{67}$$

$$\sum_{n=0}^{\infty} B_n = B(0) + L^{-1}\left(\alpha_B \sum_{n=0}^{\infty} B_n\right) - L^{-1}\left(\frac{\alpha_B}{K_2} \sum_{n=0}^{\infty} G_n\right) - L^{-1}\left(\gamma_3 \sum_{n=0}^{\infty} B_n\right) \tag{68}$$

$$\sum_{n=0}^{\infty} S_n = S(0) + L^{-1}(i) - L^{-1}\left(\beta \sum_{n=0}^{\infty} D_n\right) - L^{-1}\left(d_1 \sum_{n=0}^{\infty} S_n\right) \tag{69}$$

$$\sum_{n=0}^{\infty} E_n = E(0) + L^{-1}\left(\beta \sum_{n=0}^{\infty} D_n\right) - L^{-1}\left((\sigma + d_2) \sum_{n=0}^{\infty} E_n\right) \tag{70}$$

$$\sum_{n=0}^{\infty} I_n = I(0) + L^{-1}\left(\sigma \sum_{n=0}^{\infty} E_n\right) - L^{-1}\left(\phi \sum_{n=0}^{\infty} I_n\right) \tag{71}$$

$$\sum_{n=0}^{\infty} F_n = F(0) + L^{-1}\left(\rho \sum_{n=0}^{\infty} I_n\right) - L^{-1}\left(\gamma_3 \sum_{n=0}^{\infty} F_n\right) \tag{72}$$

The non-linear terms are derived with the help of the Adomian polynomial which are given below,

$$P = \sum_{n=0}^{\infty} A_n;\ B^2 = \sum_{n=0}^{\infty} G_n;\ BP = \sum_{n=0}^{\infty} J_n;\ P^2 = \sum_{n=0}^{\infty} C_n;\ SF = \sum_{n=0}^{\infty} D_n$$

where,

$$A_n = \sum_{k=0}^{n} H_k P_{n-k};\ G_n = \sum_{k=0}^{n} B_k B_{n-k};\ J_n = \sum_{k=0}^{n} B_k P_{n-k};\ C_n = \sum_{k=0}^{n} P_k P_{n-k};\ D_n = \sum_{k=0}^{n} S_k F_{n-k}$$

On expanding the series and integrating we get the approximate analytical expression as given in Equations (17-24).

Application of Variational Iteration Method

The general form of a correctional function is,

$$y_{n+1}(x) = y_n + \int_0^x \lambda\{Ly_n(s) + N\widetilde{y_n}(s) - g(s)ds\}$$

where λ is a Lagrangian multiplier and is expressed as $\lambda(\eta) = \frac{(-1)^n}{(n-1)!}(\eta - t)^{n-1}$and here n is the highest order of the differential equation. For our system as the highest order is 1, the lagragian multiplier becomes -1. Based on this the correctional function of the system is,

$$H_{n+1}(t) = H_0 + \int_0^t (\alpha - \beta H_n P_n - \gamma_1 H_n)\, ds \tag{73}$$

$$I_{n+1}(t) = I_0 + \int_0^t (\beta H_n P_n - \delta I_n - \theta I_n) ds \tag{74}$$

$$P_{n+1}(t) = P_0 + \int_0^t \left(\alpha_P P_n \left(1 - \frac{P_n}{K_1}\right) - \pi B_n P_n - \gamma_2 P_n\right) ds \tag{75}$$

$$B_{n+1}(t) = B_0 + \int_0^t \left(\alpha_B B_n \left(1 - \frac{B_n}{K_2}\right) - \gamma_3 B_n\right) ds \tag{76}$$

$$S_{n+1}(t) = S_0 + \int_0^t (i - \beta S_n F_n - d_1 S_n)\, ds \tag{77}$$

$$E_{n+1}(t) = E_0 + \int_0^t (\beta S_n F_n - \sigma E_n - d_2 E_n)\, ds \tag{78}$$

$$I_{n+1}(t) = I_0 + \int_0^t (\sigma E_n - \phi I_n)\, ds \tag{79}$$

$$F_{n+1}(t) = F_0 + \int_0^t (\rho I_n - d_3 F_n)\, ds \tag{80}$$

And then, when $n = 0$, we arrive at the approximate analytical expression as given from Equations (25-32).